

Three-Dimensional Shape Representation in Monkey Cortex

Margaret E. Sereno,^{1,2,3} Torsten Trinath,²
Mark Augath,² and Nikos K. Logothetis²

¹Department of Psychology
1227 University of Oregon
Eugene, Oregon 97403

²Max Planck Institute for Biological Cybernetics
Spemannstrasse 38
72076 Tübingen
Germany

Summary

Using fMRI in anesthetized monkeys, this study investigates how the primate visual system constructs representations of three-dimensional (3D) shape from a variety of cues. Computer-generated 3D objects defined by shading, random dots, texture elements, or silhouettes were presented either statically or dynamically (rotating). Results suggest that 3D shape representations are highly localized, although widely distributed, in occipital, temporal, parietal, and frontal cortices and may involve common brain regions regardless of shape cue. This distributed network of areas cuts across both “what” and “where” processing streams, reflecting multiple uses for 3D shape representation in perception, recognition, and action.

Introduction

Converging evidence from anatomical, physiological, and lesion studies have suggested that there are two functional processing streams in primate visual cortex: (1) a ventral stream analyzing form and color information (the “what” pathway; Ungerleider and Mishkin, 1982) and (2) a dorsal stream analyzing motion and spatial information (the “where” or “how” pathway; Ungerleider and Mishkin, 1982; Goodale and Milner, 1992). It is problematic how the analysis of 3D shape fits into this conceptualization because 3D shape percepts can arise from multiple cues, some of which necessarily involve processing in areas of the “where” pathway (e.g., structure from motion) and others in areas of the “what” pathway (e.g., shape from texture and shading). In addition, multiple brain regions use 3D shape representations for varying purposes ranging from recognizing objects to grasping them. Our results, which were obtained by using fMRI in anesthetized monkeys, suggest that 3D shape representations (1) are widely distributed in occipital, temporal, parietal, and frontal cortices and (2) may involve common regions regardless of shape cue.

An essential component of primate visual function is the ability to extract and represent 3D shape and depth from information in 2D retinal images. While 3D form perception has been relatively well studied with behavioral, computational, and, more recently, functional imaging techniques in humans (e.g., Malach et al., 1995;

Ishai et al., 1999; Kourtzi and Kanwisher, 2000), there has been only a handful of physiological studies on the topic (e.g., Taira et al., 1990; Bradley et al., 1998; Janssen et al., 2000). We investigate brain mechanisms underlying the ability to perceive 3D shape from a variety of cues in the image using high-resolution fMRI in anesthetized monkeys and computer-generated 3D objects to obtain optimal stimulus control. Our goal is to localize 3D shape representation in the monkey brain and thereby determine whether or not object shape specified by different cues is computed in the same or different parts of the brain.

Previous fMRI studies in monkeys demonstrating high-resolution, stimulus-induced focal activation of visual cortex (e.g., Logothetis et al., 1999) have used stimuli designed to produce maximal activation, e.g., biologically significant stimuli (faces, figures) or dynamic stimuli rich in contrast, texture, and color. In the present study, stimuli are constructed to isolate individual shape cues resulting in relatively small, gray-scale images of objects with uniform color and texture. We first investigated the extent and nature of activation for this highly constrained stimulus set defined by different cues. Next, we used control stimuli (cf. Logothetis et al., 1999) to isolate areas specifically sensitive to 3D shape, focusing primarily on shape defined by motion cues and secondarily on shape from texture. It is well established in psychological studies that motion parallax (the relative movement of parts of an object; Wallach and O’Connell, 1953; Rogers and Graham, 1979) and texture gradients (Gibson, 1950; Cutting and Millard, 1984) can produce powerful impressions of depth and surface shape. This study represents a novel attempt to define the network of visual areas in the monkey brain responsible for these shape constructions. Our results suggest the presence of a widely distributed functional architecture for 3D shape that could serve not only as a guide for electrophysiological experiments, but also prompt a reexamination of function in a number of cortical areas. Preliminary reports of these findings have appeared previously (M.E. Sereno et al., 2000, Soc. Neurosci., abstract; M.E. Sereno et al., 2001, Soc. Neurosci., abstract).

Results

Candidate Areas for 3D Shape Processing

The goal of the first set of experiments was to define candidate areas for 3D shape processing by comparing brain activity resulting from presentation of objects defined by one or more cues with that caused by presentation of a blank screen. Although activation in early visual areas (V1, V2, V3) was expected due to elementary visual processes (edge and motion detection, figure-ground segregation, etc.), we were particularly interested in observing the extent and location of activation in more anterior regions. The only fMRI report of activation in anterior regions of the monkey brain, i.e., anterior superior temporal sulcus (STS) and frontal cortex, was for stimuli consisting of faces and animal figures (Logo-

³Correspondence: margaret.sereno@tuebingen.mpg.de

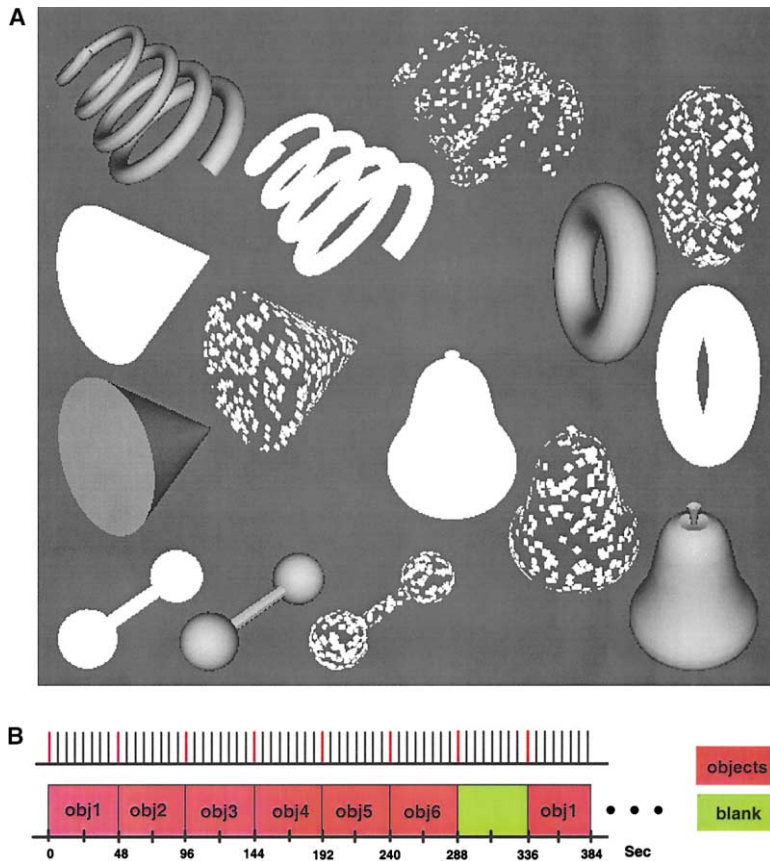


Figure 1. Example Stimuli and Paradigm

(A) Computer-generated objects are created with the goal of sampling a wide range of possible 3D shapes and surface curvatures. Identical 3D shapes were rendered with shading, random dots, texture, or as silhouettes. Examples of shaded, textured, and silhouetted objects are shown.

(B) Experimental protocol (objects versus blanks). Six objects are presented sequentially (48 s per object) followed by 48 s of blank screen (test object conditions are shown in red and control blank condition in green). Acquisition of an EPI volume (which takes 6 s for 13- and 15-slice volumes) is represented as a single vertical bar on the time line shown at the top. Red vertical bars represent images acquired during the first 6 s of each epoch that are discarded in order to obtain a steady state signal.

thetis et al., 1999). In contrast, high-contrast rotating checkerboard patterns produced robust activation in the lateral geniculate nucleus, striate, and early extrastriate cortex (including motion areas in the STS), but not more anterior regions of the temporal lobe or frontal cortex (Logothetis et al., 1999).

A variety of computer-generated 3D objects (geometrical shapes, organic forms) defined by shading, random dots, texture elements, or silhouettes were presented either dynamically (rotating) or statically with small displacements in the x-y plane (mimicking microsaccades that keep the image from fading on the retina). Figure 1A illustrates several examples rendered with shading, texture, and silhouettes (see also supplemental movie online at <http://www.neuron.org/cgi/content/full/33/4/635/DC1>). A wide range of surface shapes was used to investigate how the visual system represents surface configurations. In one paradigm, each object of a total of six objects was presented for 48 s, and this object sequence was followed by a 48 s blank screen (Figure 1B). The entire sequence was repeated four times within a scan. Objects within a scan were defined by the same cue (e.g., shading). Up to four scans (one cue per scan) were run in a given experiment.

Results from these six experiments (comparing objects to blanks) showed significant activation not only in early visual areas as expected, but also in parts of the STS (MT, the middle temporal area; FST, the floor of the STS; mid to anterior STS, lower and upper banks; and anterior STS, lower bank) and the AMTS (anterior

medio-temporal sulcus), suggesting involvement of multiple stages of processing of 3D form beginning in area V1 and continuing to the most anterior portions of the temporal lobe. Other areas of activation were found in the parietal and frontal cortices, as well as the lateral fissure. Dynamic (rotating) shaded objects were particularly effective stimuli, causing significant activation in the noted regions in most of the animals tested. Figure 2A shows typical results from experiments in which activation for six rotating shaded-object stimuli (rotated continuously about one of two diagonal axes) was compared to activation for a blank gray screen. The first three panels of Figure 2A illustrate activation in the STS for one animal subject. Significant activation ($p < 0.01$, corrected for multiple comparisons $p_{emc} < 0.00000023$ and corresponding critical threshold at z score = 5.17) is depicted in shades of red, orange, and yellow. The sagittal section in the first panel reveals four significant regions of activation in the STS. The yellow cross-hairs pinpoint activation on the lower bank of the anterior portion of the STS. The graph illustrates the percent signal change from baseline averaged over four repetitions for this region of interest. The second and third panels mark activation in the mid to anterior portion of the STS and the FST, respectively. Activation in the mid to anterior portion of the STS often occurred on both the lower and upper banks. Posteriorly in the STS, there is also activation in area MT (the most posterior region of STS illustrated in the sagittal section of the first panel).

Aside from occipital cortex and the STS, other regions

with significant activation include the AMTS, IPS (intraparietal sulcus), frontal cortex, and lateral fissure. Activation is shown in the AMTS (Figure 2A, fourth panel) and also in LIP (the lateral intraparietal area; Figure 2A, fifth panel) for another animal subject ($p < 0.01$, $p_{cmc} < 0.00000014$, and $z = 5.26$). In the frontal lobe, cross-hairs pinpoint activation on the anterior bank of the arcuate sulcus in the FEF (frontal eye field; Figure 2A, sixth panel). Anteriorly, another region of activation is located on the inferior prefrontal convexity ventrolateral to the principle sulcus (area 12) (see horizontal section of panel 6). Finally, two somatosensory areas in the lateral fissure were significant, both of which can be seen in the sagittal section of Figure 2A, second panel; the more posterior region is also visible on the right side of the coronal section of the figure.

Importantly, objects defined by different cues caused activation in similar areas of cortex. Figure 2B illustrates the results of an experiment comparing activation for objects defined by three static cues (shaded, textured, and silhouetted objects) and a dynamic cue (rotating random-dot objects). Significant activation occurred in early visual areas, parts of the STS, and the AMTS for either type of cue. Each object was presented with eight different initial orientations during a 48 s epoch (orientations were generated from random rotations about one of two diagonal axes). Random-dot objects were rotated, and objects defined by the other three cues were jittered for 6 s. All four cues caused activation in the same regions of the STS (Figure 2B). Regions of significant activation ($p < 0.01$, $p_{cmc} < 0.00000016$, and $z = 5.24$) are depicted in color. The panels in Figure 2B depict four different regions with significant activation in the STS: anterior STS, lower bank; mid to anterior STS, lower bank; area FST; and area MT. The yellow cross-hairs were positioned over two of these regions (mid to anterior STS and area MT). The top and bottom portions of each panel show activation from objects defined by static (shading, texture, silhouettes) or dynamic (random dot) cues, respectively. For each anatomical region, static cue activation overlaps dynamic cue activation.

Areas Sensitive to 3D Structure from Motion and Stationary Texture Gradients

The next set of experiments involved construction of control stimuli in order to isolate areas specifically sensitive to 3D structure. Control stimuli were created by reorganizing (e.g., scrambling) individual cue gradients. The same local information was preserved, but disruption of the cue gradient across the image led to a loss of an impression of depth. We report here on three experiments examining shape from motion parallax using dynamic random dots and one experiment examining shape from texture.

Motion Control Experiment 1

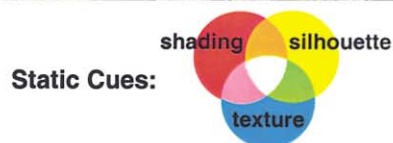
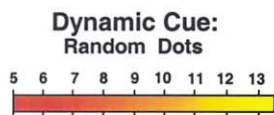
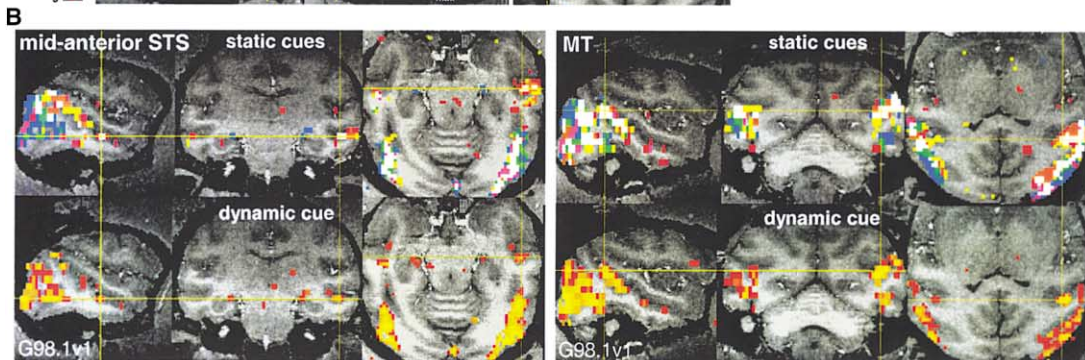
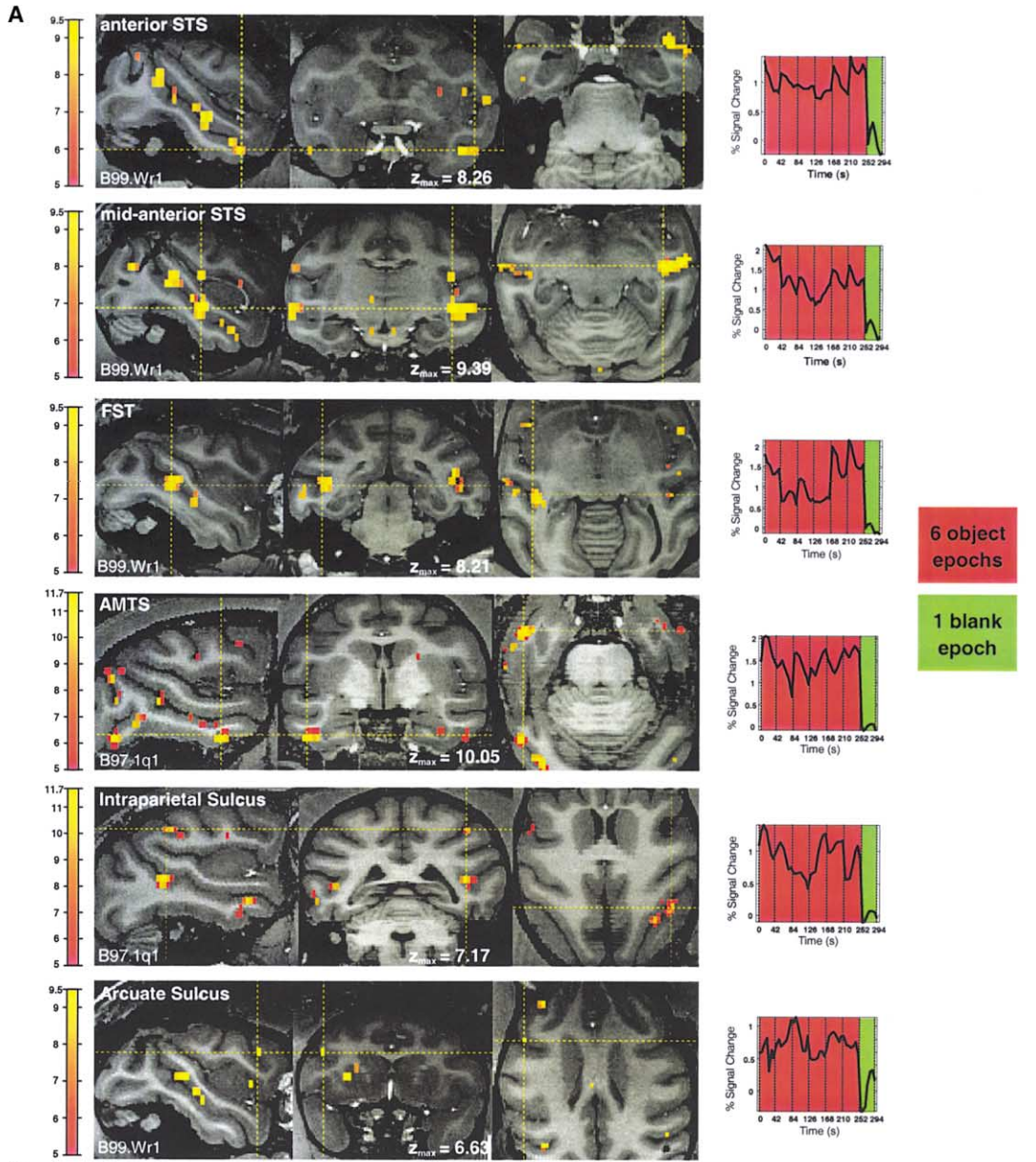
In the first motion control experiment, control stimuli for rotating random-dot objects were constructed by repositioning object dots in 3D space, rotating each dot through an arbitrary angle about the object's axis of rotation (Figure 3A). While the dots in intact and scrambled versions of each object have exactly the same motion trajectories (although with different starting posi-

tions), the intact object is seen as rotating with a clearly defined surface, while the scrambled object appears as a rotating but ill-defined volume of independently moving dots (see supplemental movie online at <http://www.neuron.org/cgi/content/full/33/4/635/DC1>).

Eight rotating intact objects were presented one after the other (for 6 s each) during a 48 s epoch, followed in similar fashion by eight scrambled controls. At the risk of increasing signal variability, we chose objects with different shapes to determine areas sensitive to shape in general. Within a scan, intact and scrambled epochs alternated four times (Figure 3C). Slices were positioned parallel to the STS. There were no movement artifacts with anesthesia, paralysis, and head restraint. The scan was repeated 15 times, and the resulting images were averaged. A paired t test was performed to compare activity in the two states ($p < 0.00001$ and $z = 4.41$).

A comparison of intact versus scrambled objects revealed greater activation for intact than scrambled rotating objects in a multitude of cortical regions in the two monkey subjects tested (C99 and E00). Significant activation in the temporal lobe included four regions of the STS (MT; FST; mid to anterior STS, lower and upper banks; and anterior STS, lower bank) and the AMTS (Figure 4A). Regions of significant activation in occipital cortex included areas VP (ventral posterior area), V2 (visual area 2), and V3 (visual area 3) (Figure 4B). Active regions in the IPS included several regions of LIP (lateral intraparietal cortex) and an area in the posterior portion of the sulcus (possibly LOP, the lateral occipital parietal zone) (Figure 5A). Because the 13 horizontal slices used in these experiments did not completely cover the frontal lobe, two additional monkey subjects were run (B00 and K00) using 15 and 18 slices (at 6 and 7 s image acquisition times), respectively, oriented horizontally to the Frankfurt zero plane, covering the frontal lobes. Results showed significant activation in area 12 of the inferior prefrontal convexity, as well as two regions in the FEF of the arcuate sulcus in one monkey subject (B00) (Figure 5B). In addition, there was an active region in cortex at the junction of parietal and occipital lobes (possibly area V3A) (Figure 5A), as well as activity in many previously identified regions of occipital cortex, the STS, and parietal cortex. Regions of significant activation for the four monkey subjects are summarized in Table 1. Functional activation was plotted on the reconstructed cortical surface of one monkey subject (E00) to aid in the visualization of activated areas (Figure 6). Figure 6 depicts activation in the lateral view of the folded (Figure 6A) and inflated (Figure 6B) right and left hemispheres, and the dorsolateral view of the inflated (Figure 6C) right and left hemispheres. To facilitate area identification, Figure 6D compares activation on the flattened right hemisphere (see right side of figure) to a schematic representation of visual areas defined anatomically (based on anatomical maps from Felleman and Van Essen, 1991; Lewis and Van Essen, 2000; and Van Essen et al., 2001; see left side of figure).

The specification of area location was based on anatomical criteria (see Felleman and Van Essen, 1991; and Lewis and Van Essen, 2000, for reviews). Specifically, locations are as follows: V2 on the posterior banks of the lunate and inferior occipital sulci; V3 on the fundus



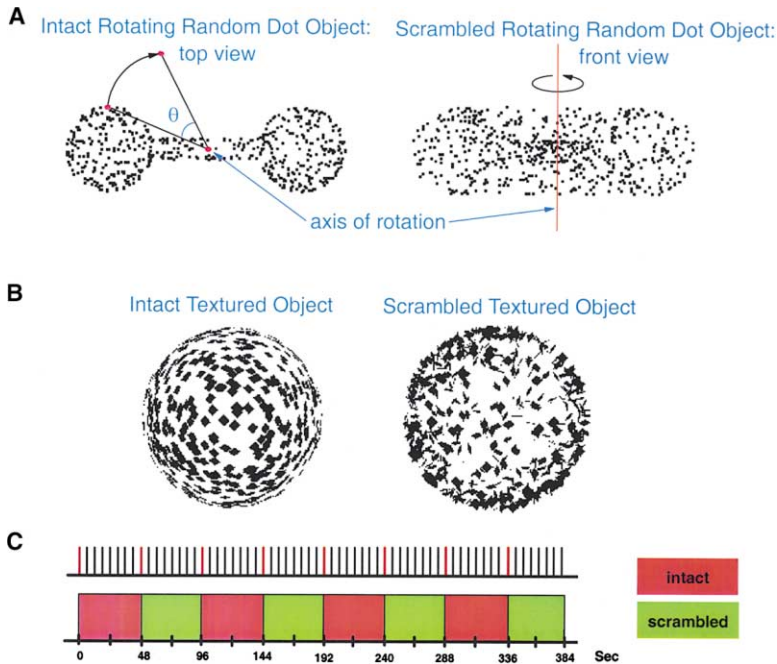


Figure 3. Stimuli and Paradigm for Experiments Isolating Areas Sensitive to 3D Structure from Motion and Shape from Texture Gradients

(A) Construction of dynamic random dot control stimuli. The left portion of the figure illustrates the top view of an intact barbell object. A scrambled control object is generated by rotating each dot on the object's surface (through an arbitrary angle, θ , about the object's axis of rotation) to a new position creating a 3D cloud of dots. The right portion of the figure illustrates the scrambled barbell object in front view. During the experiment, both intact and scrambled objects are continuously rotated about the vertical axis of rotation.

(B) Construction of static textured objects and their controls. An intact textured object, an ellipsoid, is depicted to the left; its scrambled control (created by scrambling texture element positions) is depicted to the right.

(C) Experimental protocol. Eight intact rotating random dot objects (or 24 jittering intact textured objects) are presented sequentially in a 48 s epoch (given a 6 s acquisition time for 13- and 15-slice volumes) followed by eight scrambled rotating random dot (or jittering textured) controls also in a 48 s epoch. The intact test conditions (shown in red) and scrambled control conditions (shown in green) alternated four times.

and anterior bank of the lunate sulcus; VP on the fundus and anterior bank of the inferior occipital sulcus; MT on the fundus and posterior bank of the STS; FST on the floor of the STS, anterior to MT; an area in the parietal-occipital junction (possibly V3A); LOP on the posterior portion of the IPS; LIP on the dorsal portion of the lateral bank of the IPS (possibly LIPd); and FEF on the anterior bank of the arcuate sulcus. Other areas are self descriptive (e.g., anterior STS, mid to anterior STS, AMTS, inferior prefrontal convexity).

In order to assess the consistency in location of areas between monkey subjects, we measured distances between the temporal poles and the centers of the four regions of activation in the STS of the first two monkey subjects. The average distances between the four spots and each temporal pole were: 39 mm (MT), 32 mm (FST),

21 mm (mid to anterior STS), and 16 mm (anterior STS). The average difference in position between corresponding areas in the two monkey subjects was 2.8 mm (greatest difference was 4 mm); the average distance between areas in the two hemispheres of one monkey was 2.6 mm (greatest difference was 3 mm).

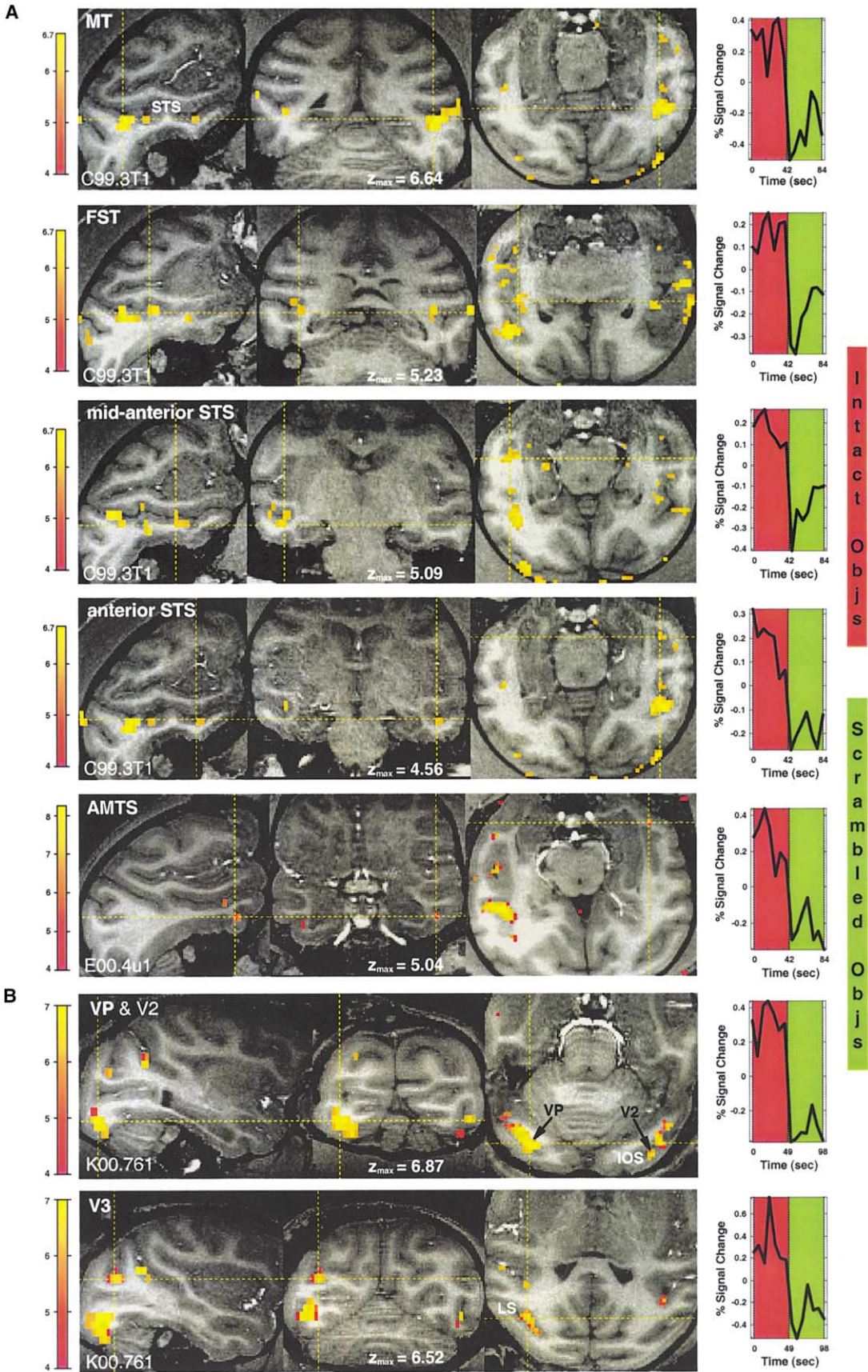
Texture Control Experiment 1

Shape from texture arises from changes in the shape of projected texture elements on a 3D object (the foreshortening of texture elements caused by a surface tilting away from an observer). Control stimuli were constructed by scrambling the texture gradient (texture element positions were swapped; see Figure 3B). Twenty-four intact, textured objects (three views of eight objects) were presented sequentially (2 s per view) during a 48 s epoch followed in similar fashion by 24 scram-

Figure 2. Activation Maps and Signal Modulation for Experiments Isolating Candidate Areas for Shape Processing

(A) Sagittal (left), coronal (middle), and horizontal (right) sections showing activation for rotating shaded objects versus blank screen. The yellow cross-hairs pinpoint activation in different parts of the brain. For a given section (e.g., horizontal), each dashed yellow line represents the positioning of the two other sections (coronal and sagittal). Regions of significant activation are depicted in shades of red, orange, and yellow, corresponding to particular z score values (refer to the color bar to the left of each panel). The graphs depict percent signal change (averaged over four repetitions) for significant voxels located in a contiguous region around the intersection point of the cross-hairs. The maximum z score for each of these regions is indicated at the bottom of each panel. Because the first 6 s of each epoch was discarded (to avoid cross-talk due to the hemodynamic delay), 42 s epochs are plotted (object epochs are shown in red and blank epochs in green). The monkey subject (e.g., B99) and experiment (e.g., W1) are indicated at the lower left of each sagittal section. The depicted regions of interest are: STS (including anterior STS, lower bank; mid to anterior STS, lower and upper banks; FST; and MT; see first three panels), AMTS (4th panel), intraparietal sulcus (area LIP; 5th panel), and inferior arcuate sulcus (FEF; 6th panel).

(B) Experiment involving four cues (static shaded, textured, and silhouetted objects and rotating random dot objects) versus blanks. Sagittal, coronal, and horizontal sections (from left to right) show activation for all four cues in the STS. In the top portion of each part of the figure, significant activation for the three static cues is depicted in different colors (see the key at the lower right of the figure); voxels with significant activation for two cues are depicted in pink, green, or orange and, for all three cues, in white. The bottom portion of each part of the figure shows significant regions of activity for rotating random dot stimuli. The level of significance is indicated by the color bar which shows z score values (at the lower left of the figure). The yellow cross-hairs are positioned over two of four regions of the STS with significant activation for all four cues.



bled controls. All objects moved with small displacements in the x-y plane. Within a scan, intact and scrambled epochs alternated four times (Figure 3C). In two monkey subjects (D97 and B00), 15 slices were positioned parallel to the STS; in two others (B01 and J00), 18 slices were oriented horizontally to the Frankfurt zero plane, covering the frontal lobes. The scan was repeated 20 times and the resulting images were averaged. A paired t test was performed to compare activity in the two states ($p < 0.001$ and $z = 3.28$).

Surprisingly, a comparison of intact versus scrambled objects revealed greater activation for intact textured objects in many of the same areas found in the motion control experiment, albeit at a slightly lower signal strength (see Table 1 and Figure 7 for results). Significant activation in the temporal lobe included four regions of the STS (MT; FST; mid to anterior STS, lower and upper banks; and anterior STS, lower bank) and the AMTS (Figure 7, panels 2–4). Regions of significant activation in occipital cortex included areas VP and V3 (Figure 7, panel 1). Other regions included LIP (Figure 7, panel 5), V3A (panel 6), FEF (panels 4 and 6, sagittal sections), prefrontal cortex below the principal sulcus (panel 4, sagittal section), parts of the lateral fissure (panel 3, sagittal section), and the amygdala (panel 7). Activation of the amygdala was also often present in the motion control experiments (including subject B01, also run in motion control experiment 2).

Motion Control Experiments 2 and 3

In motion control experiment 1, rotating objects with intact speed gradients appear as curved surfaces, whereas rotating control objects with scrambled gradients look like surfaceless, ill-formed volumes. The impression of volume in scrambled objects is due to motion parallax (the presence of a variety of dot speeds with opposite directions of motion); the lack of surface impression may result from local speed incoherence. Although control in experiment 1 is maintained for intact and scrambled objects by means of identical dot motions, other differences exist. One difference is local speed coherence—the speed of neighboring dots in intact objects is much more similar than those in the scrambled objects. A second difference is contour shape. While both types of objects have a bounding contour defined by a region of white dots against a black background, the intact object's boundary changes over time, possibly giving rise to 3D shape information.

We performed two additional experiments (motion control experiments 2 and 3) to control for speed coherence and occluding contour differences (see Figures 8A–8C) with three conditions: condition A, 3D surfaces;

condition B, coherent motion control; and condition C, incoherent motion control. In experiment 2, condition A (3D surfaces) consisted of eight opaque, random dot spheres, each rotating in one of eight directions; condition B (coherent motion), consisted of random dot stimuli positioned behind a circular aperture moving in one of eight directions (alternatively accelerating and decelerating from 0°/s to the maximum 2D dot velocity in the sphere in condition A); and condition C, dots moving in one of eight directions with speeds ranging from 0 to the maximum sphere 2D velocity. Figure 8A illustrates the instantaneous velocity field of stimuli in the three conditions at two time points during the 8 s presentation of a single stimulus. In experiment 3, condition A (3D surfaces) consisted of eight extended surfaces that rocked back and forth about the y axis. The example surfaces shown in Figure 8B are depicted with shading and contours for illustrative purposes. Condition B (coherent motion) consisted of an extended field of random dots moving in opposite directions every 125 frames (dot speed was incremental or decremental with each change in direction). In Condition C (incoherent motion), the speed of dots in each control stimulus ranged from 0 to the maximum 2D speed present in the corresponding surface stimulus; dot direction changed from left to right every 125 frames. Figure 8C illustrates the instantaneous velocity field of stimuli in the three conditions at two time points during the 8 s presentation of a single stimulus (time point two occurs after the stimuli have changed direction). In both experiments, stimuli in all three conditions have equivalent boundaries with similar dot motions, but different spatiotemporal organizations (A, speed gradient; B, uniform speed; C, incoherent speed).

Eight rotating sphere or rocking surface stimuli were presented one after the other for eight s each during a 64 s epoch (condition A), followed in similar fashion by 8 coherent speed controls (condition B) and eight incoherent speed controls (condition C). Within a scan, 3D surface and control epochs were presented four times each in pseudo-random order (ABCBCACABACB; each condition following the other two conditions twice). Twenty slices were oriented horizontally to the Frankfurt zero plane. The scan was repeated five times and the resulting images were averaged. A paired t test was performed to compare activity in the 3D surface and coherent speed, 3D surface and incoherent speed, and coherent and incoherent speed conditions ($p < 0.0001$ and $z = 3.89$).

Results from motion control experiments 2 and 3 confirm those of experiment 1. Activation produced by 3D surfaces (objects or extended surfaces) compared to

Figure 4. Sagittal, Coronal, and Horizontal Sections Showing Areas of Activation for Intact Versus Scrambled Rotating Random Dot Objects in Temporal and Occipital Lobes

(A) Temporal lobe activation. The yellow cross-hairs are positioned over four areas of the STS (MT, FST, mid to anterior STS, anterior STS) and the AMTS.

(B) Occipital lobe activation. The yellow cross-hairs are positioned over activated areas VP and V3. Area V2 activation can be seen in the horizontal section of the first panel, on the posterior bank of the IOS. Various sulci are labeled in white: STS (superior temporal sulcus), IOS (inferior occipital sulcus), and LS (Lunate Sulcus). The graphs depict percent signal change from the scan mean (averaged over four repetitions) for significant voxels located in a contiguous region around the intersection point of the cross-hairs. The maximum z score for each of these regions is indicated at the bottom of each panel. Because the first 6 s (for scans with 13 or 15 slices, subjects C99 and E00) or 7 s (for scans with 18 slices, subject K00) of each epoch were discarded, 42 or 49 s epochs are plotted (object epochs are shown in red and scrambled epochs in green).

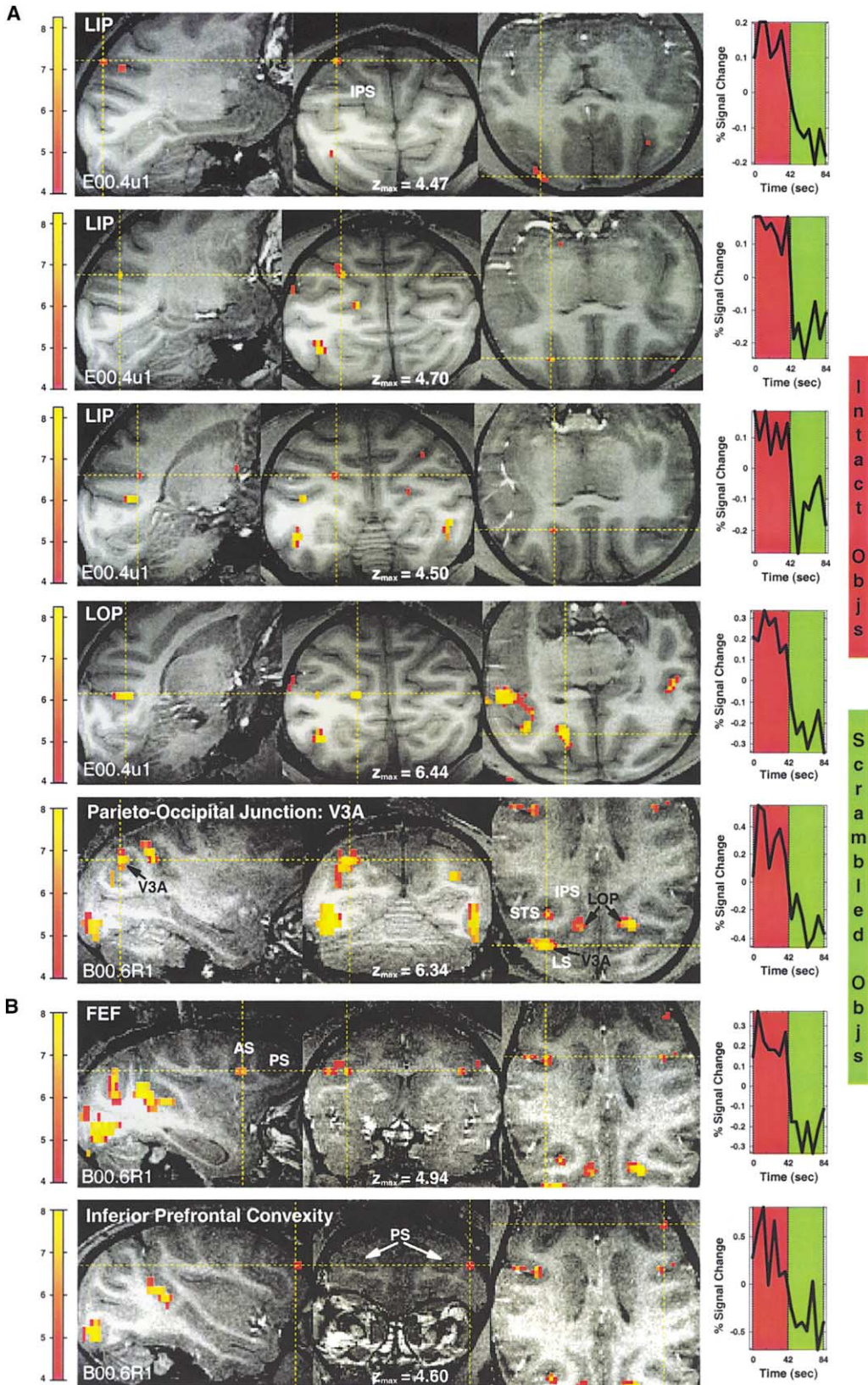


Figure 5. Sagittal, Coronal, and Horizontal Sections Showing Areas of Activation for Intact Versus Scrambled Rotating Random Dot Objects in Parietal and Frontal Lobes

The yellow cross-hairs are positioned over activated areas of (A) intraparietal sulcus (LIP and LOP), parieto-occipital junction (area V3A) and (B) frontal cortex (one of two foci of activity in the FEF on the anterior bank of the arcuate sulcus and area 12 on the inferior prefrontal

either control condition was greater in many of the previously identified areas in occipital, temporal, parietal, and frontal cortices (see Table 1). The set of areas showing a significant difference in activation for 3D surfaces versus coherent motion and 3D surfaces versus incoherent motion was either very similar (e.g., subject B01.a21, motion control experiment 2) or else surfaces versus coherent speed produced differences in more areas (e.g., subject N00.aj1, motion control experiment 3). The surfaces versus incoherent speed comparison often produced differences in the same areas as surfaces versus coherent speed but at a lower critical threshold. In the areas of interest, 3D surfaces produce the greatest activation, followed by incoherent speed (specifying a volumetric, surfaceless stimulus), and then coherent speed (specifying a flat surface). This conforms with the results of t tests comparing incoherent and coherent speed conditions that showed differences (greater activation for incoherent dot motion) in the following areas: subject N00.aj1 (anterior STS, mid-ant STS, lateral fissure, LIP, and FEF), subject C01.9T1 (anterior STS), and subject B01.a21 (anterior STS).

Discussion

Our results indicate activity in numerous cortical visual areas for 3D shape analysis with a variety of cues. Previous monkey fMRI work (Logothetis et al., 1999) has shown that biologically relevant 3D shape stimuli (monkey faces and bodies), but not dynamic 2D checkerboard stimuli, activate more anterior cortical regions (anterior STS and prefrontal cortex). Here, we show that uniformly textured and colored 3D shape stimuli defined by cues (shading, texture, silhouettes, and dynamic random dots) with very different image features also activate regions beyond striate and early extrastriate cortex including areas in temporal, parietal, and frontal lobes. Investigation of 3D shape from motion parallax and static texture gradients, using experimental designs to isolate 3D shape processes, further suggested that 3D shape-specific processing involves at least the following areas: V2, VP, and V3 in occipital cortex; MT, FST, mid to anterior STS (lower and upper banks); anterior STS (lower bank) and the AMTS in temporal cortex; V3A in the parieto-occipital junction; LOP and LIP in the intraparietal sulcus; and two frontal lobe regions (the FEF on the rostral bank of the arcuate sulcus and area 12 on the inferior prefrontal convexity ventrolateral to the principle sulcus). Two experiments (motion control experiments 2 and 3) controlled for motion coherency and external contour shape by comparing intact speed gradients specifying object or surface 3D structure to coherent and incoherent speed control stimuli with identical external boundary shapes, further demonstrating preferential activation of these areas to speed gradients specifying 3D surface shape. The areas defined by the

motion and texture control experiments represent a subset of areas found using the less stringent multiple cue paradigm (shaded, random dot, silhouetted, textured objects versus blanks), demonstrating notable consistency across paradigms and monkey subjects. The presence of this activity in anesthetized monkeys also suggests that a great deal of processing of 3D shape is “automatic,” occurring without attention or awareness.

Importantly, our results suggest that 3D shape processing from different cues occurs in areas associated with both “what” and “where” pathways. For example, it is not the case that structure-from-motion is computed in motion areas or parietal cortex while shape-from-texture is computed in temporal cortex. Instead our findings begin to demonstrate many common, overlapping processing sites for shape from both *static* and *dynamic* cues, offering a possible basis for cue-invariant 3D shape representation. The presence of 3D shape representations in parietal, temporal, and frontal regions no doubt reflects alternate cognitive requirements for perception, recognition, and action (Logothetis and Sheinberg, 1996).

We discuss our results in terms of the brain regions involved, touching on several notable features: (1) 3D shape processing in the temporal lobe involving multiple areas of the STS and the AMTS, but not lateral TE, (2) the presence of 3D shape representations in numerous other brain regions, many of which are thought of as part of the “where” pathway (parietal cortex), (3) activation for objects and faces in monkeys versus humans, and (4) cue-invariant representation.

Temporal and Occipital Lobe Activation

Areas of the temporal lobe involved in the representation of visual objects include TEO and TE (Logothetis and Sheinberg, 1996). We consistently find activation on the lower bank of anterior STS (areas TEa and TE_m) for 3D shape stimuli defined by static or dynamic cues. The lower bank of anterior STS receives inputs from more caudal parts of STS including areas MT, MST, and FST (Seltzer and Pandya, 1989a, 1994; Boussaoud et al., 1990; Morel and Bullier, 1990), from TEO on the lateral surface (Seltzer and Pandya, 1978; Distler et al., 1993), from the ventro-anterior portion of lateral TE (Saleem et al., 2000), as well as parietal cortex (Andersen et al., 1990; Seltzer and Pandya, 1994). Cells in anterior STS respond preferentially to complex stationary patterns including faces and hands (Baylis et al., 1987). A recent neurophysiological study (Janssen et al., 2000) reported a concentration of neurons selective for 3D shape-from-stereo located on the lower bank of anterior STS, but not on the lateral surface of IT cortex (lateral TE). Our results further suggest that the lower bank of the anterior portion of the STS contains cells coding for 3D shape from texture and motion parallax as well, and we also do not see significant activation on the lateral surface

convexity). Various sulci are labeled in white: IPS (intraparietal sulcus), STS (superior temporal sulcus), LS (lunate sulcus), AS (arcuate sulcus), and PS (principal sulcus). The graphs depict percent signal change from the scan mean (averaged over four repetitions) for significant voxels located in a contiguous region around the intersection point of the cross-hairs. The maximum z score for each of these regions is indicated at the bottom of each panel. Because the first 6 s of each epoch were discarded, 42 s epochs are plotted (object epochs are shown in red and scrambled epochs in green).

Table 1. Motion and Texture Control Experiments

Visual Areas	Seven Motion Experiments							Four Texture Experiments							
	C99.3T1 Exp1	E00.4u1 Exp1	B00.6R1 Exp1	K00.761 Exp1	B01.a21 Exp2a	B01.a21 Exp2b	C01.9T1 Exp3a	C01.9T1 Exp3b	N00.aJ1 Exp3a	N00.aJ1 Exp3b	Motion Exps: Total	D97.4f1	B00.5o1	B01.bs1	J00.bt1
V2	+	+	+	+	+	+	-	-	-	-	(5/7) 71%	+	-	-	-
VP	na	+	+	+	+	+	+	+	-	-	(5/6) 83%	+	+	-	+
V3	+	-	+	+	+	+	+	+	-	-	(5/7) 71%	+	+	-	+
MT	+	+	+	+	+	+	+	+	+	+	(7/7) 100%	+	+	+	+
FST	+	+	+	+	+	+	+	+	+	+	(7/7) 100%	+	+	+	+
Mid-Ant STS	+	+	+	+	+	+	+	+	+	+	(7/7) 100%	+	+	+	+
Ant STS	+	+	-	+	+	+	+	+	-	-	(6/7) 86%	+	+	+	+
AMTS	-	+	na	+	+	+	+	+	-	-	(4/6) 67%	+	+	+	+
POJ(V3A)	-	-	+	+	+	+	+	+	+	+	(5/7) 71%	-	+	+	+
LOP	-	+	+	+	-	+	-	+	-	-	(4/7) 57%	-	+	+	+
LIP	+	+	+	+	+	+	+	+	+	+	(7/7) 100%	+	+	+	+
FEF	na	na	+	+	+	+	+	+	+	+	(4/5) 80%	na	na	+	+
PF: Inf	na	na	+	-	-	-	+	-	-	-	(3/5) 60%	na	na	+	+
Convex															

Areas of significant activation for seven monkey subjects (C99, E00, B00, K00, B01, C01, and N00) in the motion control experiments ($p < 0.0001$) and four monkey subjects (D97, B00, B01, and J00) in the texture control experiments ($p < 0.001$).

Animal subjects and experiments are listed in the column headings. There were three different motion control experiments: Exp1, intact versus scrambled objects; Exp2a, spheres versus coherent speed translation; Exp2b, spheres versus incoherent speed translation; Exp3a, surfaces versus coherent speed translation; Exp3b, surfaces versus incoherent speed translation.

Cortical areas are listed as row headings: V2 (visual area 2), VP (ventral posterior area), V3 (visual area 3), MT (middle temporal area), FST (floor of the STS), Mid-Ant STS (mid to anterior STS), Ant STS (anterior STS), AMTS (anterior medio-temporal sulcus), POJ (V3A) (parieto-occipital junction, visual area 3A), LOP (lateral occipital parietal zone), LIP (lateral intraparietal area), FEF (frontal eye field), PF: Inf Convex (prefrontal cortex: inferior convexity).

Plus symbols (+) indicate areas with significant activation for experimental versus control conditions of each experiment.

Minus symbols (-) indicate areas without significant activation.

For the motion experiments, the percentage of animals with significant activity in each area is listed in the column under the heading "Motion Exps: Total" (only the data from Exp2a and Exp3a are considered for animal subjects B01, C01, and N00).

(TE or TEO). Consistent with the known convergence of inputs to the STS region described above, this report demonstrates overlapping activations for 3D shapes rendered by several distinct cues.

We also find activation in the upper bank of mid to anterior STS (area TPO). The upper bank of rostral STS receives converging projections from parietal, prefrontal, and superior temporal regions (Seltzer and Pandya, 1978, 1989a, 1989b; Selemon and Goldman-Rakic, 1988; Boussaoud et al., 1990; Seltzer et al., 1996). This area is polymodal, containing cells responsive to visual, auditory, and/or tactile stimuli (Desimone and Gross, 1979; Bruce et al., 1981; Baylis et al., 1987; Mistlin and Perrett, 1990). It contains cells that are sensitive to motion (Bruce et al., 1981; Baylis et al., 1987), including movements of the human body (Perrett et al., 1985; Oram and Perrett, 1994, 1996) and also cells that respond to faces (Baylis et al., 1987). The region of activation we have identified may thus contain polymodal representations (e.g., visual and tactile) of 3D shape.

Other regions of the temporal lobe with pattern- and shape-selective responses are areas TE, TEO, and the AMTS. Neurons in the AMTS in monkeys have been shown to be selective for specific views of 3D objects (Logothetis and Pauls, 1995). The ability of monkeys in that study to recognize and distinguish exemplars from a class of similar 3D objects may critically depend on 3D shape analysis. It is somewhat surprising that we did not observe any activation in lateral TE or TEO for 3D object shape given the significant degree of pattern selectivity of cells in these regions. One explanation is that pattern selectivity in these areas is not specific for 3D form. Indeed, experiments in lateral TE have demonstrated minimal differences in the neural responses to 3D objects and simplified 2D versions of those objects (Kobatake and Tanaka, 1994; Tanaka, 1996) or to 3D stereo shapes and 2D versions of those shapes (Janssen et al., 2000). These findings raise questions about the exact function of these areas. Perhaps neurons in lateral TE and TEO code for distinguishing features of objects defined by rich variations in color, pattern, or texture. The stimuli used in our experiments are lacking in such surface features and, therefore, may be less than optimal stimuli for these areas. Another possibility is that activity in these regions is particularly reduced due to anesthesia. Electrophysiological and fMRI experiments in alert monkeys in the future will clarify these issues.

A previous monkey fMRI study comparing monkey faces with scrambled versions of the same images found activation in regions of the STS and frontal cortex similar to those in the present study (Logothetis et al., 1999). These results are intriguing because they suggest that face and 3D object processing in the monkey occur in nearby (possibly overlapping) regions. In contrast, studies of static (e.g., Malach et al., 1995; Kourtzi and Kanwisher, 2000; Moore and Engel, 2001) and dynamic (Orban et al., 1999; Paradis et al., 2000) 3D object shape using fMRI in humans do not show involvement of the STS in 3D shape analysis. Instead, studies of object processing suggest that a region beginning in lateral occipital cortex and extending into ventral temporal cortex (the LOC or "lateral occipital complex") is important for the analysis of static object shape (see Grill-Spector et al., 2001, for a review), while studies of dynamic shape

implicate regions in occipital and parietal lobes (Orban et al., 1999; Paradis et al., 2000), as well as human MT+ (Orban et al., 1999). The question of whether the LOC is specifically involved in processing static 3D shape information is under debate with one study finding equivalent responses to 3D line drawings and 2D outline silhouettes of the same objects (Kourtzi and Kanwisher, 2000) and another reporting an increase in activity within the LOC when images of objects are perceived as 3D volumes rather than 2D shapes (Moore and Engel, 2001). The results from the human fMRI studies differ from ours in (1) the location of many of the areas, pointing to potentially significant anatomical differences in object processing in humans and monkeys, and (2) the overall number of areas, a notable finding possibly due to higher spatial resolution and minimal motion artifacts in the present study.

The results we present here show that static and dynamic 3D shape is represented in both ventral and dorsal streams. Cue invariance in the temporal lobe has been previously demonstrated for 2D shapes. Some cells in lateral TE are selective for 2D shape defined by differences in luminance, texture, or motion (Sáry et al., 1993). We reported activity for static 3D shape (defined by texture) in many of the same regions found for dynamically defined 3D shape including regions of the STS (MT, FST, mid and anterior STS; M.E. Sereno et al., 2000, *Soc. Neurosci.*, abstract), as well as parietal and prefrontal regions (M.E. Sereno et al., 2001, *Soc. Neurosci.*, abstract). This was later confirmed in humans in a study investigating object-selective responses to flat static objects (defined by silhouettes or stereo disparity), 2D translating objects, and shaded objects in human MT/MST (Kourtzi et al., 2002) corroborating our results in area MT, although with much smaller reported effects.

Several other surprising results are noted. The robust activation of area MT in the rotating random dot control experiments indicates that MT neurons do more than simply detect local motion (Zeki, 1974; Maunsell and Van Essen, 1983; Albright, 1984; Newsome et al., 1989; Sereno, 1993) or represent depth order in ambiguous rotating stimuli (Bradley et al., 1998; Sereno and Sereno, 1999) showing a clear preference for intact motion gradients that define 3D surfaces. In fact, significant activation for 3D objects/surfaces was demonstrated in areas MT and FST in all monkey subjects in the motion control experiments, as well as the texture control experiment (see Table 1). This finding is supported by another fMRI study in monkeys investigating areas involved in extracting structure from motion, showing activation in MT, additional foci in the STS, as well as the IPS and IOS (W. Vanduffel et al., 2000, *Soc. Neurosci.*, abstract). While no electrophysiological studies have yet shown selectivity in MT for motion gradients specifying 3D curved surfaces, one study has shown selectivity for motion gradients specifying flat moving surfaces tilted in depth (Xiao et al., 1997). Our motion data clearly predict a possible preference of neurons in areas MT and FST for 3D stimuli specified by speed gradients compared to stimuli translating with either coherent or incoherent speed. The results of the texture experiment showing greater activation in MT and FST for a 3D surface defined by texture gradients compared to scrambled control stimuli is particularly intriguing and will be

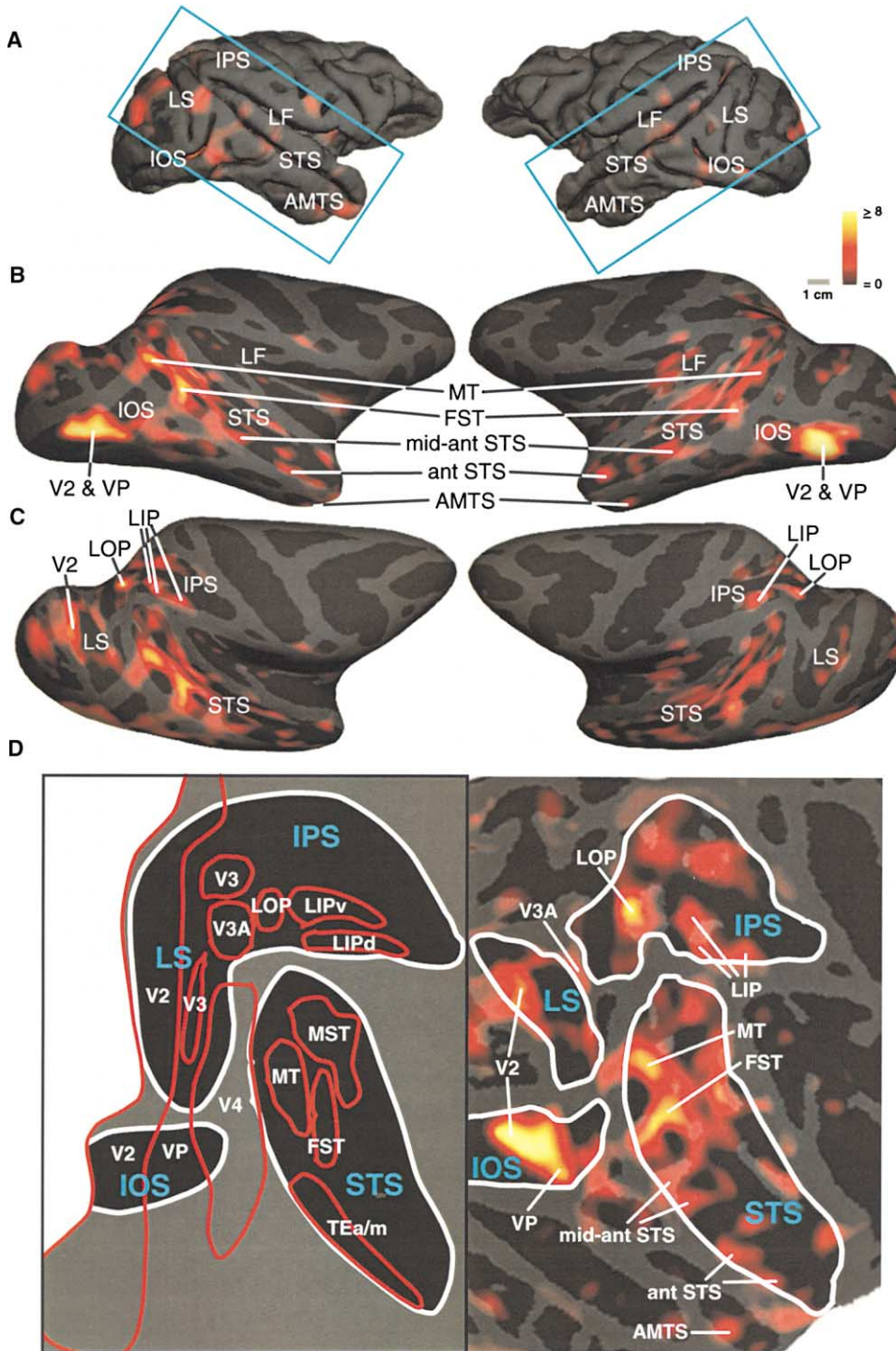


Figure 6. Cortical Surface Representation of fMRI Responses to Intact Versus Scrambled Rotating Objects (Motion Control Experiment 1) in One Subject (E00.4u1)

In this subject, data were obtained from 13 slices oriented parallel to the STS (covering most of occipital, temporal, and parietal lobes). The blue rectangles in part (A) of the figure delineate the slice volume. Areas of activation in the subject are painted onto (A) lateral views of folded right and left hemispheres, (B) lateral views of inflated right and left hemispheres, (C) dorsolateral views of inflated right and left hemispheres, and (D) flattened views of the right hemisphere comparing functionally defined areas on the right with a schematic depiction of anatomically defined areas on the left (adapted from Van Essen et al., 2001). Major sulci are labeled with white or blue letters: LF (lateral fissure), STS (superior temporal sulcus), AMTS (anterior medio-temporal sulcus), IOS (inferior occipital sulcus), LS (lunate sulcus), IPS (intraparietal sulcus). In parts (A)–(C), cortical areas are pinpointed with white lines and labeled with black letters; in part (D), they are labeled with white letters: MT (middle temporal area), FST (floor or fundus of the STS), mid-ant STS (mid to anterior STS), ant STS (anterior STS), AMTS (anterior medio-temporal sulcus), VP (ventral posterior area), V2 (visual area 2), LOP (lateral occipital parietal zone), LIP (lateral intraparietal area). The level of significance is indicated by the color bar which shows z score values.

more fully investigated with other static shape stimuli in future experiments. In addition, the activation of V3 and VP by static and dynamic cues suggests that these two areas are functionally more similar to each other than previously reported (Burkhalter et al., 1986), at least for the kinds of shape stimuli presented here (see Lyon and Kaas, 2001, for further discussion).

Parietal and Frontal Lobe Activation

Selectivity for shape has occasionally been found in regions outside occipital and temporal cortices. We find 3D shape-specific activation in several regions of the intraparietal sulcus (LIP and LOP) and parieto-occipital junction (V3A). Several electrophysiological studies also locate shape-selectivity in the intraparietal sulcus, focusing on 3D shape representation as it relates to the visual control of hand movements (Taira et al., 1990; Murata et al., 1996, 2000). When monkeys are trained to grasp real 3D objects, selectivity for the shape, size, and orientation of those objects is reported in neurons located in AIP (anterior intraparietal area). Another study, however, found that many neurons in LIP exhibit sensory shape selectivities to simple 2D geometric shapes, even when the animal performs a simple fixation task. Many units also show significant shape-dependent differences in delay-period activity in a delayed match-to-sample paradigm (Serenio and Maunsell, 1998). These results indicate that some neurons in posterior parietal cortex contribute to attending and remembering shape features in a way that is independent of intending to act or learning about shape through action. A recent study also demonstrates selectivity for stereo disparity-defined surface orientation in caudal intraparietal sulcus (Taira et al., 2000), a region probably corresponding to LOP (Lewis and Van Essen, 2000). Our results support the notion that 3D shape representation exists in parietal cortex and can be activated independent of intention or action.

In the monkey, the dorsolateral areas 9 and 46 of prefrontal cortex receive inputs from posterior parietal cortex (Petrides and Pandya, 1984), whereas ventrolateral areas 12 and 45 receive inputs from temporal areas TEO and TE (Webster et al., 1994). Consistent with neuroanatomical connections, some investigators report spatially-selective responses in dorsolateral prefrontal cortex and object-specific responses in ventrolateral cortex within the inferior prefrontal convexity (Wilson et al., 1993). One set of studies found a highly circumscribed region within inferior prefrontal cortex where neurons selectively respond to faces (O'Scalaidhe et al., 1997, 1999). Tracer injections showed that this physiologically-defined prefrontal region receives input from the ventral bank of STS (areas TEm and TEa; O'Scalaidhe et al., 1997, 1999). We also find activation for 3D objects in inferior prefrontal cortex (just below the principle sulcus). The demonstrated selectivity for faces in electrophysiological and fMRI studies and the significant activation for 3D objects in this study in anterior STS and inferior prefrontal cortex suggest that coding for faces and 3D objects in monkeys occurs in nearby, possibly overlapping regions of frontal and temporal cortices.

We find up to two foci of activation for 3D shape from

motion and texture located in the FEF of the arcuate sulcus, approximately at the level of the principle sulcus. While both regions appear to be located on the anterior bank, the more medial region is in the fundus. This region of the FEF receives converging inputs from both dorsal and ventral processing streams (Schall et al., 1995), including many of the 3D shape areas we have defined (MT, FST, lower bank and fundus of mid to anterior STS, and LIP). Separate saccadic and pursuit eye movement regions of the FEF have also been identified (see Tehovnik et al., 2000, for a review). At the level of the principle sulcus, small-amplitude saccadic eye movements are represented on the anterior bank of the arcuate sulcus and smooth pursuit eye movements to foveal targets in the fundus and posterior bank. Our results suggest that these regions of the FEF also demonstrate visual responsiveness for 3D shape. This representation of 3D shape in the FEF may be critical in guiding saccadic eye movements to different locations on the surface of an object and/or tracking features on the surface of a rotating object (Ringach et al., 1996).

Conclusions

We have defined a distributed network of areas involved in 3D shape analysis that includes areas from both "what" and "where" processing streams. This activity reflects automatic processing of 3D shape divorced from the influences of attention, memory, or intention. These representations may be used for recognizing objects, grasping them, or defining the goal of an eye movement, but they persist independent of these functions, indicating that they are also important in 3D shape representation. These activations presumably reflect the accumulation of learning about 3D object shape over a lifetime.

We have demonstrated the use of high-resolution fMRI in anesthetized monkeys to reveal a functional neuroanatomy for 3D shape analysis from both dynamic and static cues. These results can serve as a useful guide for electrophysiological experiments. In future experiments we will continue to investigate shape from shading, texture, contour, stereo disparity, and silhouettes (using more stringent control stimuli) in order to identify areas involved in cue invariance and to determine the degree of overlap for different cues and classes of shape stimuli (e.g., objects and faces). We have uncovered several important and surprising results: (1) many discrete areas are involved in 3D shape representation, (2) the same areas are active for different cues (motion and texture cues), (3) many regions beyond occipital cortex show robust activity in the anesthetized monkey for 3D shape, (4) some 3D shape areas are close to and, perhaps, overlap with face-specific regions (anterior STS and prefrontal cortex), (5) novel, perhaps unexpected, areas for 3D shape processing have been identified (caudal STS–MT and FST, parietal, FEF), and (6) a surprising lack of activation is noted in other areas (TEO, lateral TE). These results raise as many questions as they answer. The search for answers will undoubtedly clarify our understanding of visual processing in the brain.

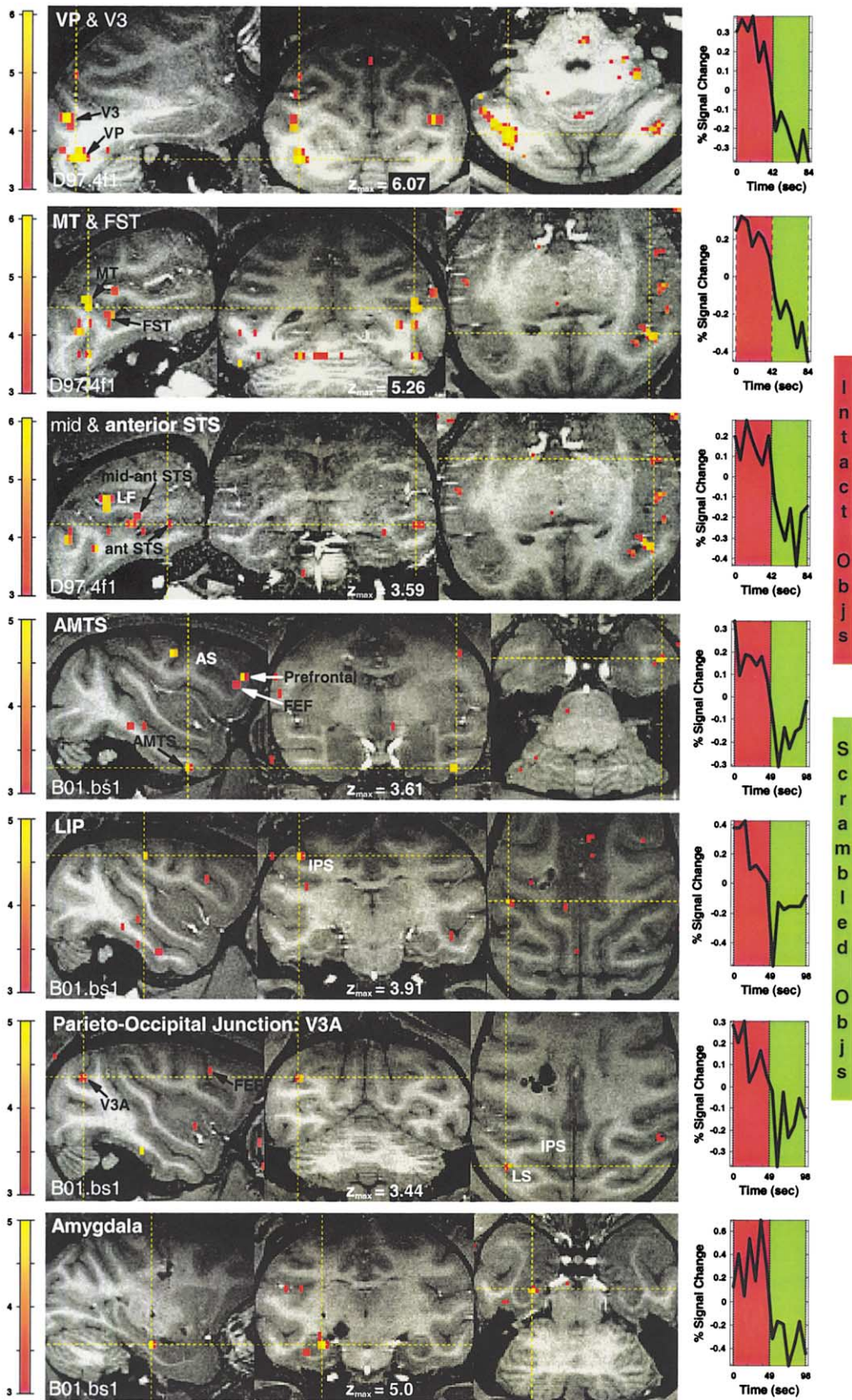


Figure 7. Sagittal, Coronal, and Horizontal Sections Showing Areas of Activation for Intact Versus Scrambled, Textured Objects in Occipital, Temporal, Parietal, and Frontal Lobes

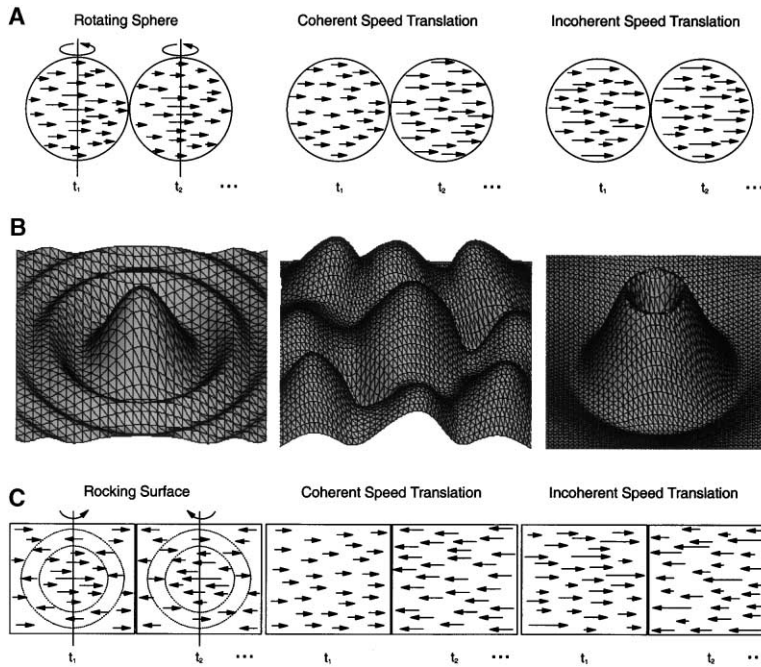


Figure 8. Stimuli Used in Motion Control Experiments 2 and 3

(A) Velocity field depiction of stimuli used in the three conditions of motion control experiment 2. The first “rotating sphere” condition contained opaque random dot spheres each rotating in one of eight different directions. The figure depicts the instantaneous velocity field of a single sphere rotating in the 0° direction at two time points. The second “coherent speed translation” and third “incoherent speed translation” conditions both consisted of random-dot stimuli positioned behind a circular aperture, each translating in one of eight directions. For each condition, the figure depicts the instantaneous velocity field of a single field of dots translating in the 0° direction at two time points. In the coherent speed condition, dot speed was manipulated so that dots alternately accelerate and decelerate from 0 to the maximum 2D velocity of the sphere stimulus. In the incoherent speed condition, dot speed was scrambled over space (in a given instant, dot speeds ranged from 0 to the maximum 2D velocity of the sphere stimulus).

(B) Example surfaces used in motion control experiment 3 depicted with shading and contours for illustrative purposes. The stimuli

were rendered with random dots, aligned in the x-y plane, and rotated back and forth through a limited 10° angle.

(C) Velocity field depiction of stimuli used in the 3 conditions of motion control experiment 3. The first “rocking surface” condition contained eight different random dot surfaces, each rocking back and forth about a vertical axis (125 frames for one direction of rotation) for 8 s. The figure depicts the instantaneous velocity field of the center portion of the leftmost surface shown in (B). The second “coherent speed translation” and third “incoherent speed translation” conditions both consisted of an extended field of random dot stimuli at two points in time, the second time point after a direction change. In the coherent speed condition, dot speed was incremented (or decremented) with each change in direction. Dots alternatively increased and decreased in steps in a range from 0 to the maximum 2D velocity of each surface. In the incoherent speed condition, dot speed in each control stimulus ranged from 0 to the maximum 2D speed present in the corresponding surface stimulus.

Experimental Procedures

This study presents 17 experiments in 13 healthy monkeys (*Macaca mulatta*) weighing 5 to 13 kg approved by the local authorities (Regierungspraesidium) in full compliance with the guidelines of the European Community (EUVD 86/609/EEC) for the care and use of laboratory animals. An abbreviated description of methods used in the experiments follows (see Logothetis et al., 1999, for complete details).

Animal Preparation

The anesthesia protocol was previously developed to ensure stress-free treatment of the animal, while, at the same time, preserving neural responses to visual stimulation. After premedication (glycopyrolate and ketamine) and insertion of an IV into the saphenous vein, anesthesia was induced (fentanyl, thiopental, and succinylcholine chloride), the trachea intubated, and the lungs ventilated. Balanced anesthesia was maintained with isoflurane in air (0.3% end-tidal) and fentanyl intravenously (3 µg per kg per hr). Muscle relaxation was achieved with mivacurium chloride (5 mg per kg per h). Lactated Ringer’s solution was given intravenously at a maximum rate of 10 ml per kg per h. Physiological parameters (pulse and

respiration rate, blood pressure, body temperature, etc.) were monitored for stability throughout the experiment. Intravascular volume was maintained by administering colloids (hydroxyethyl starch, 10–50 ml over 1–2 min as needed). After the eyes were dilated with cyclopentolate, contact lenses were used (with appropriate dioptric power for each animal) to maintain focus on the stimulus plane. The eyes were kept open and moistened with irrigating lid specula.

Visual Stimulus Generation and Positioning

The visual stimulator was a dual processor Pentium II workstation running Windows NT (Intergraph Corp., Huntsville, Alabama) equipped with two VX113 graphics subsystems. The screen resolution was reduced to 640 by 480 pixels and the frame rate to 60 Hz. All image generation was in 24 bit true-color, using hardware double buffering to provide smooth animation. The 640 × 480 VGA output was converted to a video signal (NTSC) for driving the video interface of a fiberoptic system (Avotec, Silent Vision, Florida). The field of view of the system was 30° horizontal × 23° vertical of visual angle and the focus was at 50 cm. The stimuli were presented binocularly using two independently positioned plastic, fiberoptic glasses. Alignment of the stimulus center with the fovea of each eye was achieved with the aid of a modified fundus camera. The timing of

The sagittal sections of the panels illustrate activation in areas VP and V3 (panel 1), MT and FST (panel 2), mid and anterior STS (panel 3), AMTS and frontal areas (panel 4), LIP (panel 5), parieto-occipital junction (area V3A) and FEF (panel 6), and the amygdala (panel 7). The yellow cross-hairs are positioned in the seven panels over activated areas VP, MT, anterior STS, AMTS, LIP, V3A, and amygdala, respectively. Various sulci are labeled in white: LF (lateral fissure), AS (arcuate sulcus), IPS (intraparietal sulcus), and LS (Lunate Sulcus). The graphs depict percent signal change from the scan mean (averaged over four repetitions) for significant voxels located in a contiguous region around the intersection point of the cross-hairs. The maximum z score for each of these regions is indicated at the bottom of each panel. Because the first 6 s (for scans with 15 slices, subject D97) or 7 s (for scans with 18 slices, subject B01) of each epoch were discarded, 42 or 49 s epochs are plotted (object epochs are shown in red and scrambled epochs in green).

stimulus presentation and the acquisition of images was controlled by a PC (one Pentium CPU running the QNX real-time operating system with custom-made software).

Stimuli

The objects used as stimuli were comprised of a mesh of triangle vertices, with each vertex having an associated normal vector defining the surface orientation at that point. Objects were either pre-made or created using the software package Ray Dream Studio 5 (Meta-Creations Corporation). In the latter case, the vertex information was used to compute the triangle normals. The software to present objects was written in C (utilizing OpenGL) and Tcl/Tk. Objects were rendered with random dots, texture elements, shading, or as a silhouette. They could be rotated about any axis or translated in any direction and were drawn with an orthographic or perspective projection. When rotated, the speed of rotation was 60°/sec of angular velocity; when translated (jittered in the x-y plane), the change in position averaged 0.03° of visual angle. Objects averaged 8.5° of visual angle in size. Random dot objects were created by uniformly sprinkling 450 white dots over the surface. Dot size was 0.07° of visual angle. To create a textured surface, 450 small white squares (0.6° of visual angle when facing forward) were positioned in the center of a given triangle. The vertices of each square lay on a plane orthogonal to the surface normal at that point. Shaded objects were gray in color and illuminated with a bright white directional light source (with diffuse and specular components) positioned in front of and pointing toward the object along the z-axis. Silhouetted objects were created by coloring the surface white.

In the motion control experiments 2 and 3, dot lifetime was limited to 100 frames. Dot density was equated across all conditions within each experiment. The sphere stimuli in experiment 2 subtended 10° of visual angle and rotated at 45°/sec angular velocity (with minimum and maximum 2D dot velocities of 0° and 4°/sec). The coherent and incoherent moving random dot control stimuli in experiment 2 were presented behind a 10° circular aperture; dot speeds ranged from 0° to 4°/sec. There were eight sphere-rotation and control-translation directions (0°, 45°, 90°, 135°, 180°, 225°, 270°, and 315°). Stimuli in experiment 3 were limited in extent by the viewing frame (30° in width by 20° in height). The maximum extent of surface stimuli measured from the origin ranged from 5° to 14°. Rotation speed for all surfaces was 9°/sec; maximum 2D dot speed across the eight stimuli ranged from 0.8°/sec to 2.2°/sec. Dot speed in the two random dot control conditions matched that of the surface stimuli (ranging from 0 to the maximum 2D velocity in each surface stimulus). Stimuli in all conditions switched directions of motion (left or right) every 125 frames.

MRI Data Collection

Measurements were made on a vertical 4.7 T scanner having a 40 cm diameter bore (Biospec 47/40v, Bruker Medical Inc., Ettlingen, Germany). The system was equipped with a 50 mT/m actively shielded gradient coil (Bruker, B-GA 26) of 26 cm inner diameter. A primate chair and a special transport system were designed for positioning the monkey within the magnet. During the experiment, the monkey's head was positioned with a custom-made plastic head holder previously implanted on the cranium of each animal. A Helmholtz coil allowed homogeneous excitation of most of the brain volume. The signal-to-noise ratio of this system was typically between 80:1 and 120:1. All images were acquired with a 128 mm × 128 mm field of view. T1-weighted, high-resolution (0.5 mm isotropic) anatomical images were obtained in eight segments using the 3D-MDEFT (three-dimensional modified driven equilibrium Fourier transform) pulse sequence with echo time (TE) of 4 ms, repetition time (TR) of 21.3 ms, flip angle (FA) of 20°, and inversion time (t) of 800 ms. Multislice fMRI was performed with multishot (eight segments) gradient-recalled echo planar imaging (GE-EPI). Volumes of 13 to 20 slices were collected (1 × 1 × 2 mm voxel size). Unless otherwise mentioned, horizontal sections were oriented parallel to the Frankfurt zero plane. The acquisition parameters were: TE, 20 ms; TR, 755 ms (for scans with 13 or 15 slices), 906 ms (for scans with 18 slices), and 1007 ms (for scans with 20 slices); FA, 40°; EPI-zero-phase, 4.06 ms or 20% of phase steps; pulse length (PL), 3.0 ms; spectral width (SW), 100 kHz; line acquisition time, 1.28 ms; repeti-

tion time between slices, 50.36 ms; and number of excitations per phase encode step (NEX), 1. Navigator scans were used to correct frequency, phase, and intensity fluctuations. For each scan, an auto-shim algorithm was used for tuning the linear shim coils.

MRI Data Analysis

Data were analyzed using MATLAB and the MEDx 3.0 image processing package. The multislice data were first converted into time points, then normalized, linearly detrended, and temporally denoised (using wavelet filtering). The resulting images were spatially filtered. Parametric t tests were used to generate functional maps. For the objects versus blanks experiments, activated areas were determined by selecting voxels that met an initial threshold of $p < 0.01$ subject to Bonferroni correction (resulting in a p value corrected for multiple comparisons, p_{unc} , and corresponding critical threshold, z). For the motion and texture control experiments, we selected a somewhat lower critical threshold to reduce the risk of a type II error (not detecting an activated region) for these more difficult comparisons. Functional volumes were then resampled, resliced, and superimposed on the anatomical scans. In most cases, because both scans were acquired with a volume coil during the same session, no coregistration was necessary for the fusion of the two scan types. The cortical surface maps shown in Figure 6 were generated using FreeSurfer software distributed by Massachusetts General Hospital NMR Center and CorTechs.

Acknowledgments

This work was supported by Alexander von Humboldt and McDonnell Foundation grants to M.E.S. and by the Max Planck Society. We thank Burkhard Prause, Marty Sereno, and David Sheinberg for technical assistance; and Anne Sereno and David Leopold for comments on the manuscript.

Received June 22, 2001; revised January 16, 2002.

References

- Albright, T.D. (1984). Direction and orientation selectivity of neurons in visual area MT of the macaque. *J. Neurophysiol.* 52, 1106–1130.
- Andersen, R.A., Asanuma, C., Essick, G., and Siegel, R.M. (1990). Corticocortical connections of anatomically and physiologically defined subregions within the inferior parietal lobule. *J. Comp. Neurol.* 296, 65–113.
- Baylis, G.C., Rolls, E.T., and Leonard, C.M. (1987). Functional subdivisions of the temporal lobe neocortex. *J. Neurosci.* 7, 330–342.
- Boussaoud, D., Ungerleider, L.G., and Desimone, R. (1990). Pathways for motion analysis: cortical connections of the medial superior temporal and fundus of the superior temporal visual areas in the macaque. *J. Comp. Neurol.* 296, 462–495.
- Bradley, D.C., Chang, G.C., and Andersen, R.A. (1998). Encoding of three-dimensional structure-from-motion by primate area MT neurons. *Nature* 392, 714–717.
- Bruce, C., Desimone, R., and Gross, C.G. (1981). Visual properties of neurons in polysensory area in superior temporal sulcus of the macaque. *J. Neurophysiol.* 46, 369–384.
- Burkhalter, A., Felleman, D.J., Newsome, W.T., and Van Essen, D.C. (1986). Anatomical and physiological asymmetries related to visual areas V3 and VP in macaque extrastriate cortex. *Vision Res.* 26, 63–80.
- Cutting, J.E., and Millard, R.T. (1984). Three gradients and the perception of flat and curved surfaces. *J. Exp. Psychol. Gen.* 113, 198–216.
- Desimone, R., and Gross, C.G. (1979). Visual areas in the temporal cortex of the macaque. *Brain Res.* 178, 363–380.
- Distler, C., Boussaoud, D., Desimone, R., and Ungerleider, L.G. (1993). Cortical connections of inferior temporal area TEO in macaque monkeys. *J. Comp. Neurol.* 334, 125–150.
- Felleman, D.J., and Van Essen, D.C. (1991). Distributed hierarchical processing in the primate cerebral cortex. *Cereb. Cortex* 1, 1–47.

- Gibson, J.J. (1950). *The Perception of the Visual world* (Boston, MA: Houghton Mifflin).
- Goodale, M.A., and Milner, A.D. (1992). Separate visual pathways for perception and action. *Trends Neurosci.* 15, 20–25.
- Grill-Spector, K., Kourtzi, Z., and Kanwisher, N. (2001). The lateral occipital complex and its role in object recognition. *Vision Res.* 41, 1409–1422.
- Ishai, A., Ungerleider, L.G., Martin, A., Schouten, J.L., and Haxby, J.V. (1999). Distributed representation of objects in the human ventral visual pathway. *Proc. Natl. Acad. Sci. USA* 96, 9379–9384.
- Janssen, P., Vogels, R., and Orban, G.A. (2000). Selectivity for 3D shape that reveals distinct areas within macaque inferior temporal cortex. *Science* 288, 2054–2056.
- Kobatake, E., and Tanaka, K. (1994). Neuronal selectivities to complex object features in the ventral visual pathway of the macaque cerebral cortex. *J. Neurophysiol.* 71, 856–867.
- Kourtzi, Z., and Kanwisher, N. (2000). Cortical regions involved in perceiving object shape. *J. Neurosci.* 20, 3310–3318.
- Kourtzi, Z., Bühlhoff, H.H., Erb, M., and Grodd, W. (2002). Object-selective responses in the human motion area of MT/MST. *Nat. Neurosci.* 24, 17–18.
- Lewis, J.W., and Van Essen, D.C. (2000). Mapping of architectonic subdivisions in the macaque monkey, with emphasis on parieto-occipital cortex. *J. Comp. Neurol.* 428, 79–111.
- Logothetis, N.K., and Pauls, J. (1995). Psychophysical and physiological evidence for viewer-centered representations in the primate. *Cereb. Cortex* 5, 270–288.
- Logothetis, N.K., and Sheinberg, D.L. (1996). Visual object recognition. *Annu. Rev. Neurosci.* 19, 577–621.
- Logothetis, N.K., Guggenberger, H., Peled, S., and Pauls, J. (1999). Functional imaging of the monkey brain. *Nat. Neurosci.* 2, 555–562.
- Lyon, D.C., and Kaas, J.H. (2001). Connectional and architectonic evidence for dorsal and ventral V3, and dorsomedial area in marmoset monkeys. *J. Neurosci.* 21, 249–261.
- Malach, R., Reppas, J., Benson, R., Kwong, K., Jiang, H., Kennedy, W., Ledden, P., Brady, T., Rosen, B., and Tootell, R.B.H. (1995). Object-related activity revealed by functional magnetic resonance imaging in human occipital cortex. *Proc. Natl. Acad. Sci. USA* 92, 8135–8138.
- Maunsell, J.H.R., and Van Essen, D.C. (1983). The connections of the middle temporal visual area (MT) and their relationship to a cortical hierarchy in the macaque monkey. *J. Neurosci.* 3, 2563–2586.
- Mistlin, A.J., and Perrett, D.I. (1990). Visual and somatosensory processing in the macaque temporal cortex: the role of expectation. *Exp. Brain Res.* 82, 437–450.
- Moore, C., and Engel, S.A. (2001). Neural response to perception of volume in the lateral occipital complex. *Neuron* 29, 277–286.
- Morel, A., and Bullier, J. (1990). Anatomical segregation of two cortical visual pathways in the macaque monkey. *Vis. Neurosci.* 4, 555–578.
- Murata, A., Gallese, V., Kaseda, M., and Sakata, H. (1996). Parietal neurons related to memory guided hand manipulation. *J. Neurophysiol.* 75, 2180–2186.
- Murata, A., Gallese, V., Luppino, G., Kaseda, M., and Sakata, H. (2000). Selectivity for the shape, size, and orientation of objects for grasping in neurons of monkey parietal area AIP. *J. Neurophysiol.* 83, 2580–2601.
- Newsome, W.T., Britten, K.H., and Movshon, J.A. (1989). Neuronal correlates of a perceptual decision. *Nature* 341, 52–54.
- Oram, M.W., and Perrett, D.I. (1994). Responses of anterior superior temporal polysensory (STPa) neurons to biological motion stimuli. *J. Cogn. Neurosci.* 6, 99–116.
- Oram, M.W., and Perrett, D.I. (1996). Integration of form and motion in the anterior superior temporal polysensory (STPa) of the macaque monkey. *J. Neurophysiol.* 76, 109–129.
- Orban, G.A., Sunaert, S., Todd, J.T., Van Hecke, P., and Marchal, G. (1999). Human cortical regions involved in extracting depth from motion. *Neuron* 24, 929–940.
- O’Scalaidhe, S.P., Wilson, F.A.W., and Goldman-Rakic, P.S. (1997). Areal segregation of face-processing neurons in prefrontal cortex. *Science* 278, 1135–1138.
- O’Scalaidhe, S.P., Wilson, F.A.W., and Goldman-Rakic, P.S. (1999). Face-selective neurons during passive viewing and working memory performance of rhesus monkeys: evidence for intrinsic specialization of neuronal coding. *Cereb. Cortex* 9, 459–475.
- Paradis, A.L., Cornilleau-Peres, V., Droulez, J., Van De Moortele, P.F., Lobel, E., and Berthoz, A. Le Bihan, D., and Poline, J.B. (2000). *Cereb. Cortex* 10, 772–783.
- Perrett, D.I., Hietanen, J.K., Oram, M.W., and Benson, P.J. (1985). Visual cells in the temporal cortex sensitive to face view and gaze direction. *Proc. R. Soc. Lond. B Biol. Sci.* 223, 293–317.
- Petrides, M., and Pandya, D.N. (1984). Projections to the frontal cortex from the posterior parietal region in the rhesus monkey. *J. Comp. Neurol.* 228, 105–116.
- Rogers, B., and Graham, M. (1979). Motion parallax as an independent cue for depth perception. *Perception* 8, 125–134.
- Ringach, D.L., Hawken, M.J., and Shapley, R. (1996). Binocular eye movements caused by the perception of three-dimensional structure from motion. *Vision Res.* 36, 1479–1492.
- Saleem, K.S., Suzuki, W., Tanaka, K., and Hashikawa, T. (2000). Connections between anterior inferotemporal cortex and superior temporal sulcus regions in the macaque monkey. *J. Neurosci.* 20, 5083–5101.
- Sáry, C., Vogels, R., and Orban, G.A. (1993). Cue-invariant shape selectivity of Macaque IT neurons. *Science* 260, 995–997.
- Schall, J.D., Morel, A., King, D.J., and Bullier, J. (1995). Topography of visual cortex connections with frontal eye field in macaque: convergence and segregation of processing streams. *J. Neurosci.* 15, 4464–4487.
- Selemon, L.D., and Goldman-Rakic, P.S. (1988). Common cortical and subcortical targets of the dorsolateral prefrontal and posterior parietal cortices in the rhesus monkey: evidence for a distributed neural network subserving spatially guided behavior. *J. Neurosci.* 8, 4049–4068.
- Seltzer, J.B., and Pandya, D.N. (1978). Afferent cortical connections and architectonics of the superior temporal sulcus and surrounding cortex in the rhesus monkey. *Brain Res.* 149, 1–24.
- Seltzer, J.B., and Pandya, D.N. (1989a). Intrinsic connections and architectonics of the superior temporal sulcus in the rhesus monkey. *J. Comp. Neurol.* 290, 451–471.
- Seltzer, J.B., and Pandya, D.N. (1989b). Frontal lobe connections of the superior temporal sulcus in the rhesus monkey. *J. Comp. Neurol.* 281, 97–113.
- Seltzer, B., and Pandya, D.N. (1994). Parietal, temporal, and occipital projections to cortex of the superior temporal sulcus in the rhesus monkey: a retrograde tracer study. *J. Comp. Neurol.* 343, 445–463.
- Seltzer, J.B., Cola, M.B., Gutierrez, C., Masee, M., Weldon, C., and Cusik, C.G. (1996). Overlapping and nonoverlapping cortical projections to cortex of the superior temporal sulcus in the rhesus monkey: double anterograde tracer studies. *J. Comp. Neurol.* 370, 173–190.
- Sereno, M.E. (1993). *Neural Computation of Pattern Motion: Modeling Stages of Motion Analysis in the Primate Visual Cortex.* (Cambridge, MA: MIT Press/Bradford Books).
- Sereno, A.B., and Maunsell, J.H.R. (1998). Shape selectivity in primate lateral intraparietal cortex. *Nature* 395, 500–503.
- Sereno, M.E., and Sereno, M.I. (1999). 2D center-surround effects on 3-D structure-from-motion. *J. Exp. Psychol. Hum. Percept. Perform.* 25, 1834–1854.
- Taira, M., Mine, S., Georgopolous, A.P., Murata, A., and Sakata, H. (1990). Parietal cortex neurons of the monkey related to the visual guidance of hand movement. *Exp. Brain Res.* 83, 29–36.
- Taira, M., Tsutsui, K., Jiang, M., Yara, K., and Sakata, H. (2000). Parietal neurons represent surface orientation from the gradient of binocular disparity. *J. Neurophysiol.* 83, 3140–3146.

- Tanaka, K. (1996). Inferotemporal cortex and object vision. *Annu. Rev. Neurosci.* 19, 109–139.
- Tehovnik, E.J., Sommer, M.A., Chou, I.H., Slocum, W.M., and Schiller, P.H. (2000). Eye fields in the frontal lobes of primates. *Brain Res. Brain Res. Rev.* 32, 413–448.
- Ungerleider, L.G., and Mishkin, M. (1982). Two cortical visual systems. In *Analysis of Visual Behavior*, D.J. Ingle, ed. (Cambridge, MA: MIT Press), pp. 549–586.
- Van Essen, D.C., Lewis, J.W., Drury, H.A., Hadjikhani, N., Tootell, R.B.H., Bakircioglu, M. and Miller, M.I. (2001). *Vision Res.* 41, 1359–1378.
- Wallach, H., and O'Connell, D.N. (1953). The kinetic depth effect. *J. Exp. Psychol.* 45, 205–217.
- Webster, M.J., Bachevalier, J., and Ungerleider, L.G. (1994). Connections of inferior temporal areas TEO and TE with parietal and frontal cortex in macaque monkeys. *Cereb. Cortex* 5, 470–483.
- Wilson, F.A.W., O'Scalaidhe, S.P., and Goldman-Rakic, P.S. (1993). Dissociation of object and spatial processing domains in primate prefrontal cortex. *Science* 260, 1955–1958.
- Xiao, D.K., Marcar, V.L., Raiguel, S.E., and Orban, G.A. (1997). Selectivity of macaque MT/V5 neurons for surface orientation in depth specified by motion. *Eur. J. Neurosci.* 9, 956–964.
- Zeki, S.M. (1974). Functional organization of a visual area in the posterior bank of the superior temporal sulcus of the rhesus monkey. *J. Physiol.* 236, 549–573.